PERGAMON

Vision Research 39 (1999) 2349–2360

Vision Research

Vernier judgments in the absence of regular shape information

Saumil S. Patel, Harold E. Bedell *, Michael T. Ukwade

College of Optometry, University of Houston, Houston, TX 77204-6052, USA

Received 30 December 1997; received in revised form 5 August 1998

Abstract

Vernier acuity is a form of hyperacuity in which the threshold offset between a test object and a reference object is smaller than the size of a foveal cone. Because the test and the reference objects usually have regular shapes (e.g. rectangular, triangular or circular), relatively few studies have addressed the role of shape information in determining hyperacuity thresholds. In this study, we investigated the effect of shape information on hyperacuity performance using targets of irregular shape with different skew and symmetry properties. Vernier thresholds smaller than 10 arc-sec were obtained for closely spaced asymmetric irregular-shape targets. Thresholds for dots and asymmetric irregular shapes increased with increase in center-to-center gap between the targets. Unlike dots, the thresholds for asymmetric irregular shapes also increased with target area. Although the thresholds for asymmetric irregular shapes were higher than those for dots, thresholds for *symmetric* irregular shapes were similar. Target skew below a certain level had a negligible effect on Vernier thresholds for asymmetric shapes. Our results suggest the existence of feature-independent neural circuitry that can support hyperacuity thresholds and are consistent with the use of the centroid as a primitive for relative localization.

Keywords: Vernier acuity; Hyperacuity; Shape processing; Orientation; Centroid

1. Introduction

Two mechanisms have been proposed to explain the highly precise Vernier performance that is achieved for a wide variety of target configurations and conditions. It is suggested that a more sensitive spatial-filter mechanism operates for abutting and closely spaced targets, whereas a less sensitive local-sign mechanism signals the direction of Vernier offset for widely separated targets (Westheimer & McKee, 1977a; Wang & Levi, 1994). Although it is unknown what neural computations are actually involved in analyzing Vernier offset from the outputs of spatial filters, two general approaches have been proposed. In the first, reference-based approach (Wilson 1986), the responses of an appropriate class of spatial filters represent the Vernier targets as a point in a complex space (Fig. 1a), which has dimensions such as orientation, spatial frequency, contrast, etc. The location of this point is then compared to a reference point in the same N-dimensional space based either on an internal norm, or a normative value established from the filter responses to a set of null (zero-offset) stimuli. A non-zero value from this comparison process indicates the presence of Vernier offset. The second, symmetry-based approach (Regan & Beverley, 1985; Waugh, Levi & Carney, 1993; Mussap & Levi, 1997), compares the outputs of a pair of spatial filters with symmetric preferred orientations to directly yield a signal for Vernier offset (Fig. 1b). No difference exists between the responses of symmetrically oriented spatial filters when a pair of dot targets is aligned (upper part of Fig. 1b) whereas a non-zero difference indicates the presence and the direction of misalignment.

The limited size of cortical receptive fields is assumed to preclude the efficient operation of spatial-filter mechanisms when the elements that comprise a Vernier stimulus become too widely separated. For widely-separated targets, a local-sign scheme has been proposed to signal Vernier misalignment, as illustrated in Fig. 1c. In this scheme, the individual elements of the Vernier target are localized on a neural topographic map and the map positions (i.e. local signs) of the elements are then compared. According to Levi & Waugh (1996),

* Corresponding author. Fax: +1-713-7432053.
E-mail address: hbedell@mail-gw.opt.uh.edu (H.E. Bedell)

0042-6989/99/$ - see front matter
PII: S0042-6989(98)00265-X

comparison of the individual element's local signs involves a high-level oriented filter, which they designate as a collator unit, the output of which signals the direction of Vernier offset. Clearly, a local-sign mechanism could also provide information about Vernier misalignment for closely-spaced targets but, typically, its operation will be obscured by the superior performance of more sensitive spatial-filter mechanisms.

Most previous studies of Vernier acuity used targets of regular shape such as dots, lines and chevrons (Andrews, Butcher & Buckley, 1973; Westheimer & McKee 1977b; Watt, 1984; Meer & Zeevi, 1989; McKee, 1991; Morgan, 1991; Wilson, 1991). In this study, we sought to determine whether comparably precise Vernier performance can be obtained using irregular shapes. Consider the consequences of using irregular shapes on the processing of Vernier targets by the suggested spatial-filter mechanism. First, because a Vernier configuration composed of irregular shapes contains stimulus energy at a wide range of unpredictable orientations, it becomes difficult to establish a reference for zero Vernier offset. The visual system can not have a priori knowledge of the neural pattern that represents alignment of the stimuli, nor can it easily abstract this pattern from repeated presentations, especially if the irregular shapes are varied from trial to trial. The lack of an internal

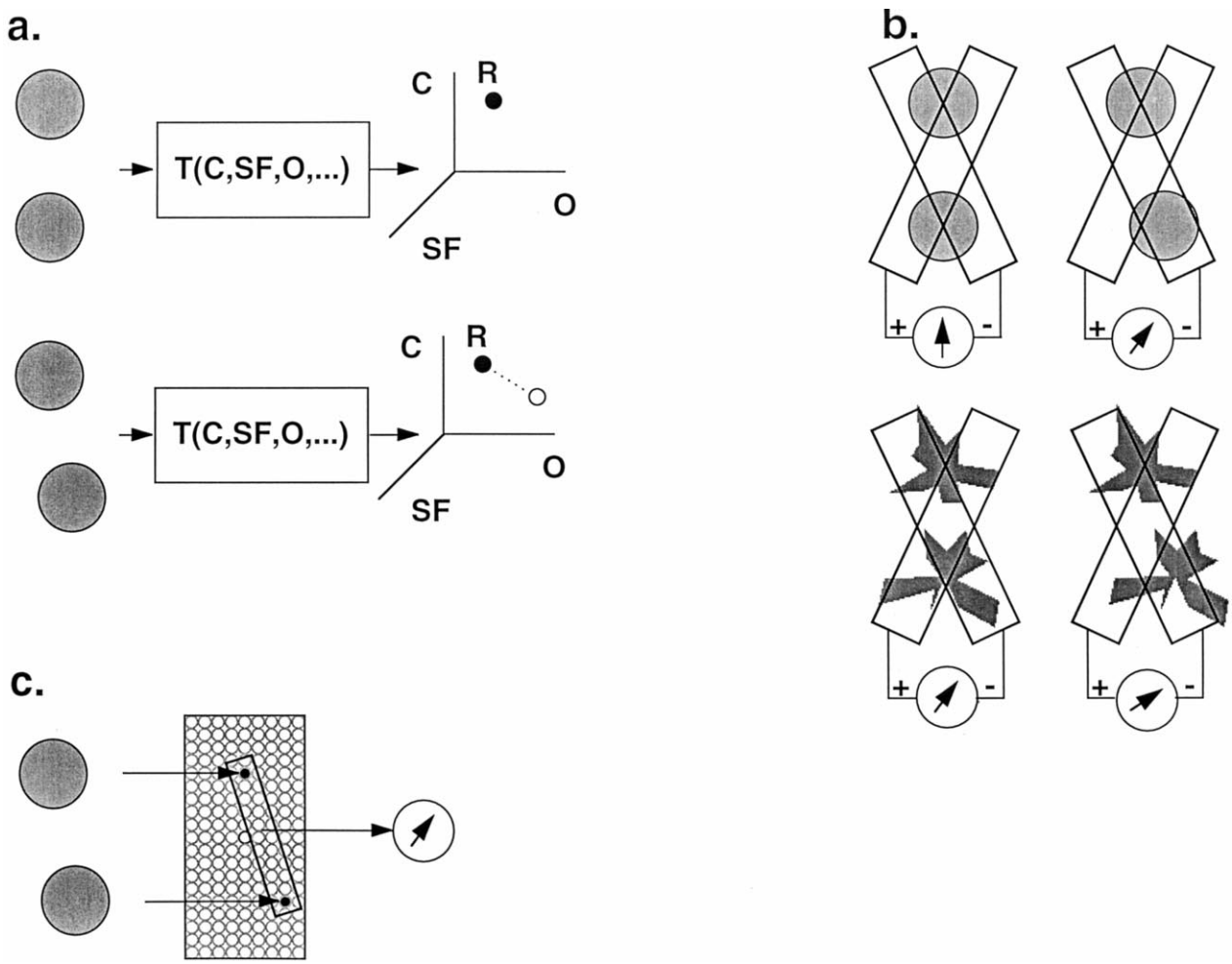

Fig. 1. Possible models of hyperacuity for Vernier offset. (a) Reference-based processing of Vernier targets. Each pair of gray circles represent a two-dot Vernier target. Rectangular boxes represent a spatial transformation function, denoted by T. The dimensions of the transformed domain include contrast (C), spatial frequency (SF), orientation (O), etc. For simplicity, consider a three dimensional transformed space of contrast (C), spatial frequency (SF) and orientation (O). The filled circle in the transformed space, denoted by R, corresponds to alignment of the Vernier target. In the lower half of this panel, misalignment of the Vernier target produces a different transform, shown by the unfilled circle. The presence and direction of Vernier offset is signaled by computing the vector length between the filled and unfilled circles. (b) Symmetry-based processing of Vernier targets. Each pair of rectangular boxes represents symmetrically oriented spatial filters. The difference between the output of these symmetric filters represents Vernier offset, as shown by the arrow below each filter pair. Responses of this comparison are shown for dots and irregular-shape targets. For asymmetric targets of irregular shape, note that a comparison between symmetric filters may signal Vernier offset, even when the centroids of the shapes are physically aligned (lower left panel). (c) Local-sign scheme for processing of Vernier targets. Each element of the target is localized independently within a position map (black dots). Position signals from this map are combined via an oriented receptive field, as indicated by the rectangular box. The output of this hypothetical collator unit indicates the presence and direction of Vernier offset.

reference should render a spatial-filter mechanism that depends on such a reference unreliable. If the irregular shapes are also asymmetric, then a spatial-filter mechanism that depends on comparing stimulus energy at pairs of symmetric orientations should also become unreliable. Vernier acuity for asymmetric irregular shapes might therefore depend on a local-sign mechanism, even for closely spaced targets.

Within the local-sign mechanism it is not clear how positions of individual components of a Vernier target are obtained for comparison. One possible spatial parameter that is often considered is the centroid of the target. The arithmetic centroid of a two-dimensional visual object can be defined as the spatial location where the sum of clockwise and counter-clockwise first-order moments of the luminance distribution is zero. If the luminance distribution of the target is homogeneous, then the centroid can be determined as the geometric centroid, and defined solely from the position of the edges. Vernier thresholds that depend on a measure such as the centroid would be expected to be largely invariant to target rotation. It is widely known that the human visual system can detect changes in the centroid of a luminance distribution that are finer than the photoreceptor matrix (Westheimer & McKee, 1977a; Morgan & Aiba, 1985). This centroid discrimination is comparable to that of a spatial filter mechanism and implies either that spatial filters are directly involved in sensing changes in target centroid (Hess, Dakin & Badcock, 1994; Badcock, Hess & Dobbins, 1996) or that the centroid of the target is computed by a separate mechanism of comparable sensitivity. A way to distinguish between the above possibilities is to selectively lower the sensitivity of one potential mechanism, for example by using targets with irregular shapes to lower the sensitivity of the spatial filter mechanism.

Ward, Casco and Watt (1985) measured the ability of subjects to judge misalignment of two abutting random dot clusters. After comparing their data to the performance of an ideal observer, they concluded that the subjects primarily used edge cues to accomplish the relative localization task. Whitaker and Walker (1988) used a similar target arrangement and reported relative localization performance in the hyperacuity range ($<$ 10 arc-sec for ~ 3 square arc-min target area). They, however, concluded that the subjects compared the geometric centroids of the test and reference targets to accomplish the task. According to Whitaker and Walker (1988), an important difference from the study by Ward et al. may be the low dot densities that Ward et al. used. Another difference between the two studies is the size of the dots. Whitaker and Walker used sub-minute dots (0.25×0.25 min) within a small rectangular region (1.7×1.7 min), whereas Ward et al. used larger dots (1.65×1.65 min) within a larger bounding rectangle (50×10 min). In both studies, thresholds depended greatly on dot density and size. An advantage of using solid irregular shapes is that interactive effects of dot density and size on Vernier thresholds are eliminated. Numerous other studies suggest that the centroid of a target is a fundamental parameter for relative and absolute localization within the human visual system (Toet, Smit, Nienhuis & Koenderink, 1988; Yakimoff, Bocheva, & Mitrani, 1990; Morgan & Glennerster, 1991; Vos, Bocheva, Yakimoff & Helsper, 1993; Bocheva & Yakimoff, 1996; Hess & Holliday, 1996; Whitaker, McGraw, Pacey & Barrett, 1996).

In this study, we compared Vernier thresholds for configurations of asymmetric irregular solid shapes, and solid dot targets of the same area. Thresholds were determined for various target areas and inter-target separations (gaps). Generalizability was evaluated by determining whether the pattern of thresholds changed when the original set of asymmetric irregular shapes underwent rotation. The influence of target symmetry and skew on Vernier thresholds was assessed in two ancillary experiments. An additive variance model is fit to the experimental data.

2. Methods

Except in the experiment involving rotated irregular shapes, the three authors participated as observers in this study. All had normal corrected acuity and binocular vision. In a normally illuminated room, the observer binocularly viewed the reflection of a computer screen (640 horizontal $\times$ 480 vertical; 14 in. diagonal; 256 gray levels) from a mirror that produced an optical distance of 980 cm. The screen was viewed through an 18-cm-diameter circular aperture. Vernier offset thresholds were determined for solid bright dots (Fig. 2a) and asymmetric irregular shapes (Fig. 2b) of three areas (8.3, 25, 37.5 square arc-min) for six *center-to-center* vertical gaps (4–46 arc-min). Targets were 60 cd/square m presented on a background of 11 cd/square m. The irregular shapes were 16-sided polygons of known centroid and area. Details about the construction and the statistical properties of the shapes are available in Appendix A. Horizontal Vernier offsets were introduced on each trial using the method of constant stimuli. In the case of irregular shapes, each Vernier trial presented a stimulus composed of two *different* shapes, each randomly picked from a pool of 18. The targets remained on the screen until the observer responded. The observers reported whether the bottom target was perceived to be offset to the left or right with respect to the top target. Vernier thresholds were the inverse slopes (50–84% correct) of the psychometric functions, fit with a cumulative Gaussian using a maximum likelihood method. In all the experiments the average of at least two threshold measurements was obtained for each condition.

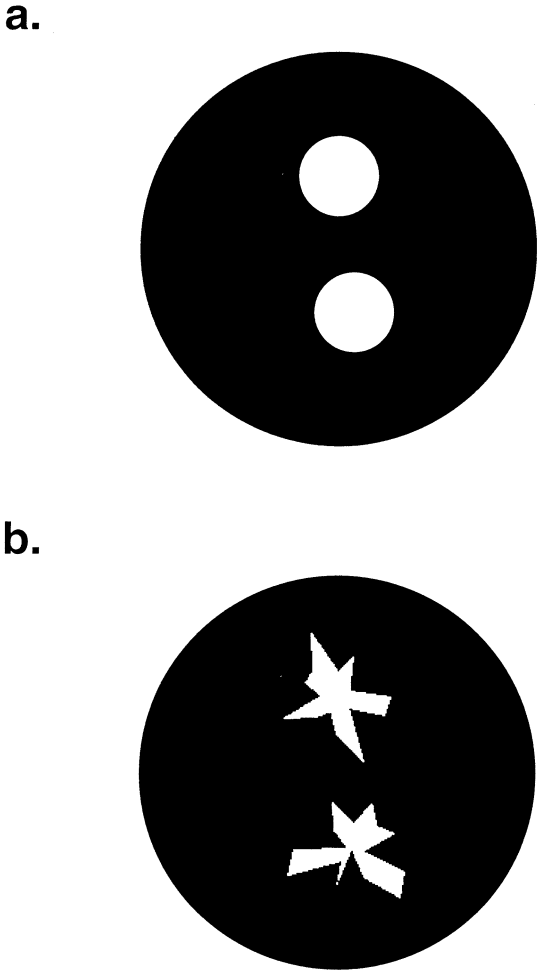

Fig. 2. Vernier test configurations. (a) Dot targets. An outer circular aperture, ~1° in diameter, eliminated references from vertical and horizontal screen edges. From trial to trial, the horizontal position of both targets was randomly jittered (max = 7.5 arc-min) to mask cues from the position of the targets with respect to the aperture. (b) Asymmetric irregular-shape targets. On each trial, different top and bottom targets were selected randomly from a pool of 18 irregular shapes. The same 18 shapes were rescaled using Adobe Photoshop to obtain the three different target areas tested. The area of the irregular shapes was the same as the corresponding-sized dots.

In a control experiment to investigate whether thresholds are invariant to stimulus rotation, all of the symmetric irregular shapes of 25 square arc-min were rotated by 90°. Thresholds were obtained for gaps of 11, 16, 26, 36 and 46 arc-min using the same protocol as described above. Only observers SP and HB participated in this experiment.

The role that target skew might have played in the main experiment was investigated in a first ancillary experiment. All of the asymmetric shapes of 25 square arc-min were rotated in steps of 1° and the angles of rotation that yielded the minimum and maximum absolute values of x-axis skew were determined. Skew was defined as the third order moment of the target's luminance distribution (Press, Flannery, Teukolsky & Vetterling, 1992). Based on these skew calculations, we created two sets of shapes. A set of 18 *large-skew* shapes included the nine rotated shapes with the largest absolute values of skew and their mirror images, obtained by imposing on each a 180° rotation. This procedure ensured that the mean skew in this set is zero, similar to the mean for the set of shapes used in the main experiment. The set of 18 *small-skew* stimuli was constructed in a similar manner, except that the nine shapes with the smallest skew were selected and then rotated by 180° to create their mirror images. Details about these two sets of stimuli, as well as for the set of 18 *medium skew* shapes used in the main experiment, are available in Appendix A. Vernier thresholds were obtained using these three sets of shapes for a target area of 25 square arc-min and a center-to-center gap of 11 arc-min. Due to changed room illumination, the targets were 52 cd/square m presented on a background of 20 cd/square m. Otherwise, the conditions remained unchanged from those in the main experiments.

A second ancillary experiment investigated how the thresholds depended upon target symmetry. Each irregular shape of the *medium skew* set was rotated in 1° steps and then divided into right and left half images. The left-half image was discarded and the right half-image was mirrored and copied to form a new left half. For each angle of rotation, this process established a new shape, which was symmetrical about the vertical axis. For each of the original asymmetric shapes, one having the same area and x, y centroid location was retained in a set of 18 *symmetric* irregular shapes. Vernier thresholds were determined using the procedures of the main experiment by sampling from this set of symmetric targets. In this experiment, the shapes had an area of 25 square arc-min and the center-to-center gap was 11 arc-min.

The statistical analyses were performed using multivariate repeated measures ANOVAs. For all the ANOVAs described in this paper, thresholds were expressed as log arc-sec, so that variances for the different conditions remained approximately equal. The P-values reported in this paper are the higher (lower) of the Huynh-Feldt and Greenhouse-Geisser corrected values for significant (insignificant) effects.

3. Results

3.1. Vernier thresholds for dots versus asymmetric irregular shapes

As shown in Fig. 3, the average Vernier thresholds for dots and asymmetric irregular shapes increase with center-to-center gap for all three target areas. Statistical analysis which included only the data for the *three gaps*

(16, 26 and 36 arc-min) tested for all three target areas indicated that the effect of gap is significant for dots ($F[2, 4] = 46.13$, $P = 0.02$) and asymmetric irregular shapes ($F[2, 4] = 19.16$, $P = 0.03$). The interactions between area and gap are not significant for dots ($F[4, 8] = 2.48$, $P = 0.21$) and asymmetric irregular shapes ($F[4, 8] = 1.12$, $P = 0.41$). Overall, for the *three gaps* and the three target areas, the average thresholds for dots (17.23 ± 1.34 [S.E.] arc-sec) are significantly ($F[1, 2] = 97.94$, $P = 0.01$) lower than for asymmetric

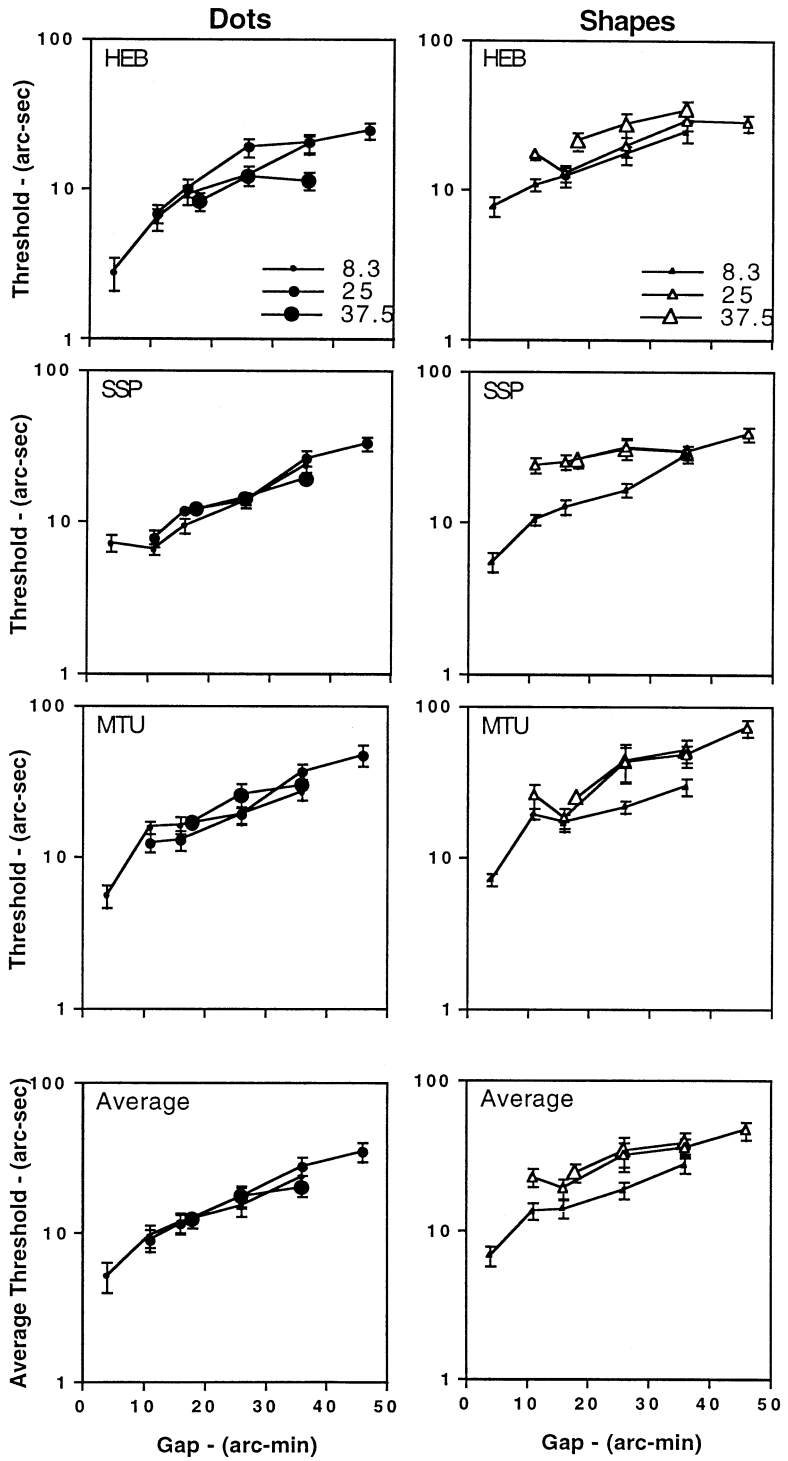

Fig. 3. The first three rows in the left (right) column show Vernier thresholds for dot (asymmetric irregular shape) targets of various areas (8.3, 25, 37.5 square arc-min) for observers HEB, SSP, and MTU. The last row shows thresholds averaged across all three observers. The thresholds are plotted as a function of the center-to-center gap which provides the only meaningful comparison between thresholds for dots and irregular shapes. The size of the symbols is proportional to the target area. In this and the following figures, the error bars represent ± 1 standard error.

irregular shapes (26.57 ± 1.95 [S.E.] arc-sec). For the smallest target area, (8.3 square arc-min), the difference between the average Vernier threshold for dots and for asymmetric irregular shapes is insignificant ($F = 5.7$, $P = 0.14$). For the smallest gap (4 arc-min), the average Vernier threshold for dots (5.1 ± 1.3 [S.E.] arc-sec) is slightly lower than that for asymmetric irregular shapes (6.7 ± 0.7 [S.E.] arc-sec). It is important to note that the observers saw all of the irregular-shape targets to have sharp edges and corners, regardless of their area. This observation indicates that optical degradation introduced by the eye did not eliminate the high-spatial frequency components that distinguish the irregular shapes from the dot targets.

As shown in Fig. 3, the average thresholds for dots are essentially area-independent ($F[2, 4] = 0.67$, $P = 0.5$). On the other hand, the average thresholds for asymmetric irregular shapes are area-dependent ($F[2, 4] = 17.28$, $P = 0.045$) and increase with target area (Fig. 3). As mentioned earlier, the interactions between gaps and areas are not significant for dots and asymmetric irregular shapes.

3.2. Rotational invariance of thresholds for asymmetric irregular shapes

For both observers tested, the thresholds for irregular shapes are rotation invariant, regardless of the gap (Fig. 4). The thresholds, averaged across observers and gaps are slightly lower for 90°-rotated irregular shapes (22.8 ± 2.5 S.E. arc-sec) than for non-rotated shapes (25.5 ± 2.3 S.E. arc-sec). However, this difference does not reach statistical significance ($F[1, 1] = 21.86$, $P = 0.13$). The interactions between gaps and rotation are not significant ($F[4, 4] = 0.1$, $P = 0.8$).

3.3. Effect of target skew on thresholds of asymmetric irregular shapes

The Vernier thresholds obtained for sets of targets with different amounts of skew are shown in Fig. 5. The effect of different shapes on Vernier thresholds is significant ($F[4, 8] = 28.5$, $P = 0.009$). The difference in threshold between dots and medium-skew asymmetric irregular shapes is significant ($F[1, 8] = 36.3$, $P = 0.009$). For the same target area (25 square arc-min) and gap (11 arc-min), the threshold difference between dots and irregular shapes in the main experiment was also significant ($F[1, 8] = 38$, $P = 0.006$). The thresholds for the sets of random shapes with medium and small amounts of skew do not significantly differ ($F[1, 8] = 0.001$, $P = 0.83$). Although the thresholds for the set of shapes with large skew are higher than those for both other sets of irregular shapes, the differences are only marginally significant (medium vs. large skew $F[1, 8] = 9.22$, $P = 0.052$; small vs. large skew $F[1, 8] = 9.1$, $p = 0.055$).

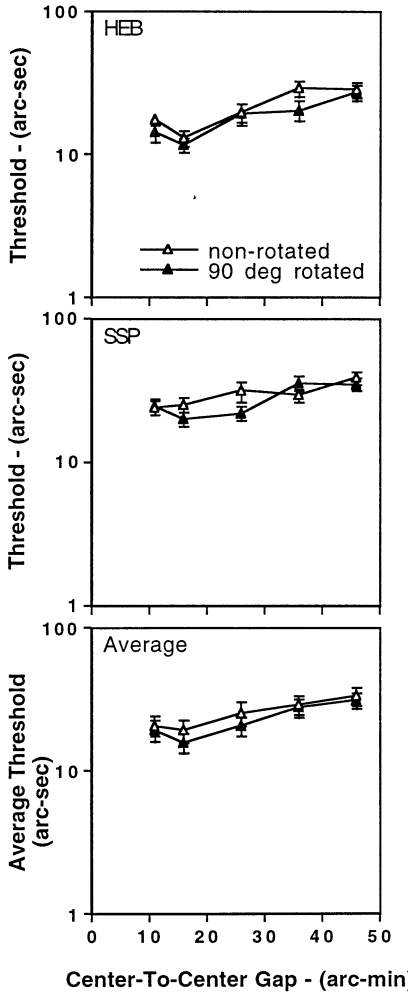

Fig. 4. Vernier thresholds for asymmetric irregular shape targets of 25 square arc-min as a function of the center-to-center gap under two conditions: non-rotated versus 90° rotated shapes. The top two panels show data for observers HEB and SSP. The bottom panel shows the data averaged across the two observers.

3.4. Effect of target symmetry on thresholds of irregular shapes

The average thresholds for the set of symmetric irregular shapes are also shown in Fig. 5. Thresholds for symmetric irregular shapes do not differ from those for dots ($F[1, 8] = 1.33$, $P = 0.25$), but are significantly lower than those obtained for all three sets of irregular shapes (compared to small skew $F[1, 8] = 24.02$, $P = 0.02$; compared to medium skew $F[1, 8] = 23.74$, $P = 0.02$; compared to large skew $F[1, 8] = 62.56$, $P = 0.004$).

3.5. Orientation angle at threshold

In Fig. 6, the data from the main experiment are re-plotted by transforming each Vernier threshold into an angular offset. Because the angular offset for dots

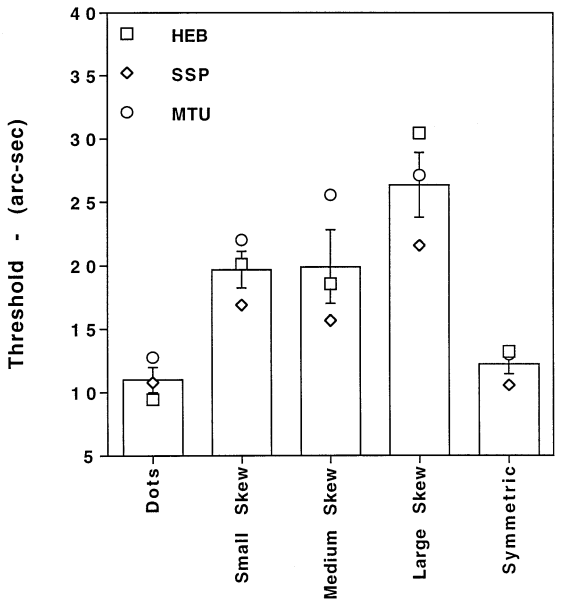

Fig. 5. Effect of target skew and symmetry on Vernier thresholds. The average thresholds ±1 S.E. are presented as a bar plot. The center-to-center gap was 11 arc-min and the area of the targets was 25 square arc-min. Thresholds for observers HEB, SSP, and MTU are superimposed on the bar plot as unfilled symbols.

can be defined in terms of the imaginary line joining either the edges or the centers of the targets, both transformations are plotted. On a log scale, the average angular offset for dots decreases approximately exponentially as the edge-to-edge (Fig. 6a) or center-to-center (Fig. 6b) gap increases, regardless of the area of the targets. The major difference between the plots in Fig. 6a, b is in the small-gap region, where the center-to-center function increases considerably less. The threshold angular offset reaches an asymptotic value of $0.74 \pm 0.04°$ [S.E.] at an edge-to-edge gap of about 20 arc-min and $0.63 \pm 0.03°$ [S.E.] at a center-to-center gap of about 25 arc-min. The average angular offset for asymmetric irregular shapes also decreases approximately exponentially as the center-to-center gap increases (Fig. 6c). However, unlike the results for dot targets, the angular offset increases systematically with target area, for all gap sizes tested. Note that, for the smallest target area (8.3 square arc-min), the threshold function for asymmetric irregular shapes is very similar to the corresponding function for dot targets (compare Fig. 6b and c), reaching an asymptotic angular offset of $0.7 \pm 0.03°$ [S.E.] at a center-to-center gap of about 25 arc-min.

3.6. Additive variance model

An additive variance model was fit to the average thresholds for dots and asymmetric irregular shapes to quantitatively analyze the effects of target area and gap. Only the data for the gap sizes (16, 26, 36 arc-min) tested for all three target areas were included in this analysis. The form of the fitted function is similar to that proposed by Morgan (1991) and is given below:

$$y = \sqrt{th_0^2 + (ag)^2 + (bx^c)^2}$$

Here, y is the threshold for targets of area x and gap g, th_0 is the minimum threshold (estimated as the threshold for the smallest dot targets at the smallest gap), a is the gain of the gap effect and b and c are the gain and the exponent of the area effect. The parameters a, b and c were obtained separately for dots and asymmetric irregular shapes by least-square minimization.

The fits of the model to the Vernier thresholds for dots and asymmetric irregular shapes are shown in Fig. 7. Thresholds for dots are independent of target area, as indicated by an extremely small value of b (0.0001).

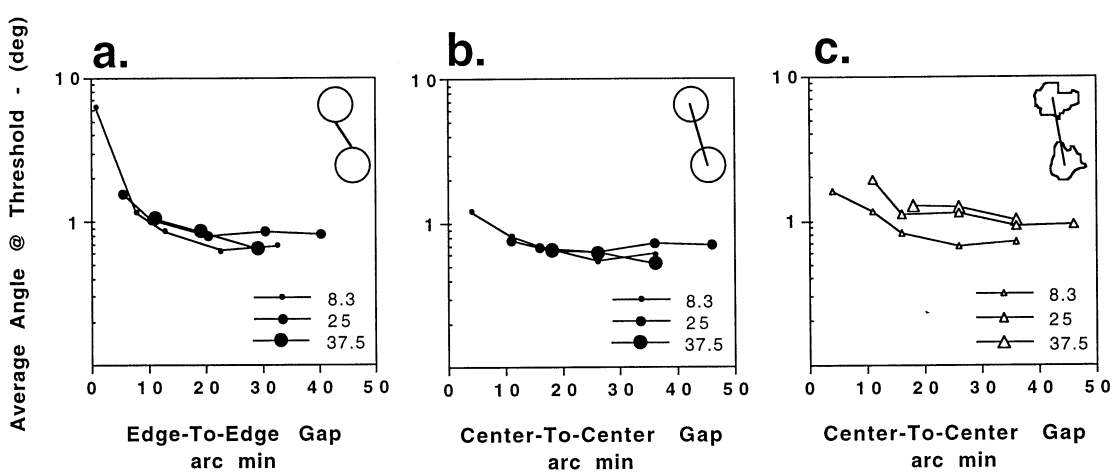

Fig. 6. The angular offset corresponding to the average Vernier offset threshold is shown for dots and asymmetric irregular shapes of various areas (8.3, 25, 37.5 square arc-min). For dots, the *angular* offset is plotted as the deviation from vertical of the imaginary line from edge to edge (a) or from centroid to centroid (b). For asymmetric irregular-shape targets, the angular offset is plotted as the deviation from vertical of the imaginary line from centroid to centroid (c).

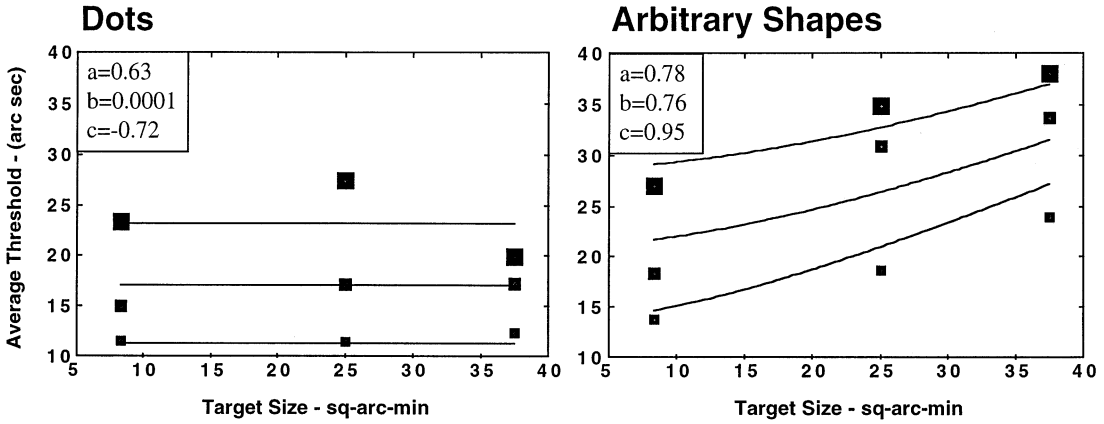

Fig. 7. Additive variance model for the effects of target gap and area on Vernier offset threshold. Each data point represents the average threshold across the three observers at each gap. The size of the symbol is proportional to the gap. The model parameters, obtained using separate least-square fits for dots and asymmetric irregular shapes, are shown in the upper left corner of each panel. The fitted curves for each gap are superimposed as solid lines.

In contrast, the thresholds for irregular shapes are *area* dependent as indicated by a value close to one (0.95). The center-to-center gap exerts similar effects on the thresholds for dots and irregular-shape targets, as indicated by the comparable values of a (0.63 for dots and 0.78 for asymmetric irregular shapes).

4. Discussion

Vernier thresholds in the hyperacuity range are possible for targets without regular shape information. It is not surprising that the thresholds for dots and asymmetric irregular shapes increase with an increase in target gap. The fact that the minimum thresholds for dots and asymmetric irregular shapes are not significantly different is an interesting result. These minimum values were obtained for the smallest center-to-center gap (4 arc-min) and for the smallest target area (8.3 square arc-min). As the mechanisms depending on internal reference and target symmetry are unlikely to play a role in determining the thresholds for asymmetric irregular shapes, it is plausible that a similarly sensitive feature-independent mechanism is responsible. In addition, our data indicate that such a mechanism is insensitive to target rotation, suggesting that a centroid-type computation may be involved in determining thresholds for asymmetric irregular shapes.

Across the larger gaps (16, 26, 36 arc-min) and target areas (8.3, 25, 37.5 square arc-min) tested, the thresholds for dots were significantly lower than those for asymmetric irregular shapes. The edge-to-edge gaps computed from the target size and center-to-center gaps of 16, 26 and 36 arc-min were greater than 10 arc-min for all sizes. Note that spatial filter mechanisms are not believed to mediate Vernier thresholds at these large gaps (Wang & Levi, 1994; Waugh & Levi 1995; but also see the last paragraph in this section). The difference in thresholds between dots and asymmetric irregular shapes may reflect the accuracy of determining the centroid for different shapes. It is conceivable that different levels of processing may be involved in determining centroids of regular shapes and irregular shapes. For well defined shapes, high-level learnt rules of geometry may be applied while for irregular shapes a noisier low-level image analysis may be involved in determining centroids. A low-level image-analysis type computation would be analogous to finding the normalized first order moments in the horizontal and the vertical directions (Levine, 1985). The fact that thresholds for dots are relatively area independent, whereas those for asymmetric irregular shapes are area dependent, also supports the idea of different centroid computation schemes. An alternative explanation of the difference in thresholds between dots and asymmetric irregular shapes may be based upon the availability of well-defined edge cues for dot target localization. For both shapes and dots the same low-level scheme may be used, however its accuracy may depend on the amount of high spatial frequency noise at various orientations in the targets. From an ideal computation standpoint, differences in spatial frequencies and orientations should not induce errors in low-level centroid computations. But the visual system is far from ideal and has limited detector resolution and presumably limited resolution for spatial frequency and orientation. Inaccurate representation of higher spatial frequencies due to the above-mentioned limitations could cause centroid computation errors in shapes that have significant energies at relatively higher frequencies. Previously, Morgan and Glennerster (1991) reported that spatial interval acuity is independent of

target size for circular discs, which they explained by noting that the uncertainty added due to increased target size is offset by a corresponding increase in number of available samples.

Thresholds obtained with asymmetric irregular shapes of small skew (S.D. ~ 0.001) were also significantly higher than those obtained with dots. The thresholds obtained with asymmetric irregular shapes of small skew were similar to those obtained for medium skew. This suggests that a factor other than skew is responsible for elevation of thresholds for asymmetric irregular shapes compared to dots. Nevertheless, Vernier performance is apparently degraded when target skew exceeds a certain critical value, as the thresholds for large-skew, asymmetric irregular shapes were higher than those for shapes with small or medium skew. As expected from a Regan–Beverley type model (Fig. 1b), the thresholds obtained using symmetric irregular shapes were indistinguishable from those for dots, suggesting that target asymmetry plays an important role in the elevation of thresholds for asymmetric irregular shapes.

For gaps greater than about 15 arc-min, the reasonably good fit of the additive variance model suggests that Vernier performance may be limited by at least two independent noise sources: (1) *area-dependent* noise in determining the location of the target centroid; and (2) *area-independent* noise in making Vernier comparisons, which increases with the gap. Compared to the *area-independent* noise, the *area-dependent* noise for regular shapes like dots is very small (Fig. 7) and can be ignored. As mentioned previously, this area independence for regular shapes may reflect a different rule-based centroid computation scheme which is minimally sensitive to an increase in area. However for asymmetric irregular shapes, *area-dependent* noise is significant and increases almost linearly with area (value of c in Fig. 7), suggesting a low-level centroid computation scheme; e.g. one that depends on the count of position detectors involved. Note that the results from previous localization studies (Jiang & Levi, 1991; Morgan & Glennerster, 1991; Vos et al., 1993) suggest that thresholds depend on the extent of the stimulus (e.g. diameter for a circular target) and not the area as found in this study. The basis for an area dependency in our data is not clear at this time but, as mentioned earlier, a low-level centroid computation scheme (Levine, 1985) would exhibit such dependency.

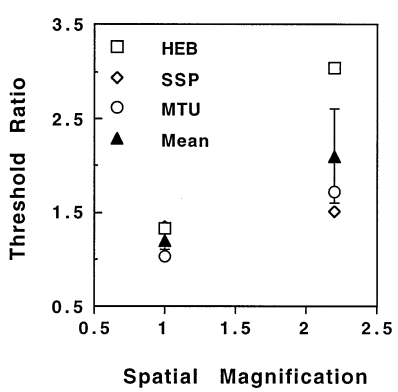

Fig. 8. Effect of spatial scale on the ratio of Vernier thresholds for asymmetric irregular shapes to those for dots. The ratio of Vernier thresholds for asymmetric irregular shapes to those for dots is plotted on the *Y*-axis for all three subjects (unfilled symbols). A filled symbol represents across subject average. The *X*-axis represents the spatial magnification. A unity magnification is assigned to the size and gap combination of 3.25 arc-min (8.3 square arc-min) and 16 arc-min, respectively. The size and gap combination of 6.9 arc-min (37.5 square arc-min) and 36 arc-min, respectively corresponds to a relative magnification of 2.25.

Although evidence exists that the local sign mechanism mediates Vernier thresholds for gaps greater than approximately 15 arc-min, the increase in thresholds with increasing gaps could also be explained by assuming that Vernier offset is detected by proportionally larger oriented spatial filters (Wilson, 1986; Burbeck, 1987; Whitaker & McVeigh 1991; Hess & Hayes 1993). According to the spatial filter model, Vernier thresholds should be higher for asymmetric irregular shapes than for dots because the irregular targets contain more orientation noise within the bandwidth of the optimal spatial filter. Orientation noise for dots is small and, in a Regan–Beverley type model (Fig. 1b), the noise for symmetric targets cancels for symmetrical orientations at each spatial frequency. Because the spectrum of the oriented noise scales with the size and separation of the targets, the spatial filter model predicts that the ratio of the Vernier threshold for asymmetric irregular shapes to that for dots should be spatial-scale invariant. Our data suggest that scale invariance fails: across subjects the average ratio of thresholds for irregular-shape versus dot targets is 1.2 ± 0.1 [S.E.] for 3.25 arc-min (8.3 square arc-min) targets separated by 16 arc-min and 2.1 ± 0.5 [S.E.] for 6.9 arc-min (37.5 square arc-min) targets separated by 36 arc-min (Fig. 8). Hence, roughly doubling the size and separation of the stimuli results in almost a doubling of the threshold ratio. Confirmation of these results by additional experiments designed specifically to investigate this issue would imply that the higher Vernier thresholds for asymmetric irregular shapes than for dots result from orientation noise that affects the centroid computation.

Acknowledgements

This work was supported by NIH grant EY05068

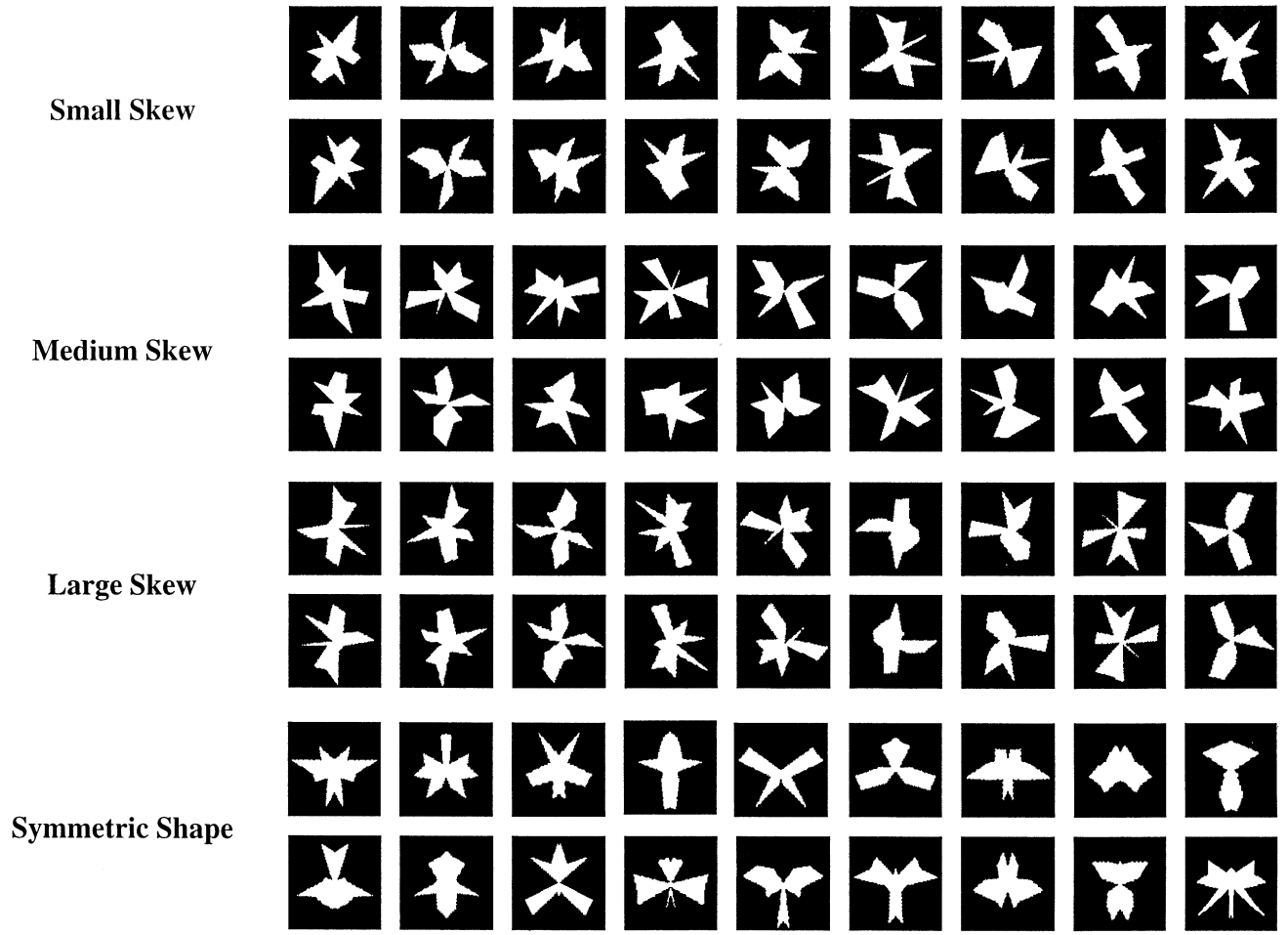

Fig. A1.

and a post-doctoral fellowship from the University of Houston ISSO. We thank Dr Dennis Levi for valuable comments. We also thank Dr Robert Hess and an anonymous referee for their useful suggestions about improving the manuscript.

Appendix A. Shape construction

The shapes were constructed inside a 100×100 pixel square pixelmap. A circle of 50 pixel radius was divided into 16 equal sectors and a random distance was marked along each of the radial lines that formed these 16 sectors. The marked points were then connected to form an irregular shape. The interior of the closed shape was filled with white and the remaining pixels remained black. An iterative process collected all the shapes that had centroid coordinates within ± 0.1 pixel of the desired coordinates of (50, 50). Out of all the shapes collected, 18 shapes with similar areas ($\sim 1800 \pm 60$ square pixels) were selected to form the initial medium skew set. These shapes were scaled up by a factor of 1.5 and scaled down by a factor of 3 to obtain the smaller and the larger areas, respectively.

A.1. Irregular shape sets

The four populations of shapes used for our experiments are shown in Fig. a1. The *medium skew* set was used in the main experiments, in which center-to-center gap and target area was varied and the results with dot targets. The *small-skew*, *large-skew* and *symmetric* shape sets were used in ancillary experiments to identify the factors responsible for differences in results between shapes and dot targets in the main experiment.

The statistical description of the population of shapes ($\sim 1800 \pm 60$ square pixels) shown in Fig. a1 is given in the following table:

Target population type	N	μ_a	σ_a	μ_{cx}	σ_{cx}	μ_{cy}	σ_{cy}	μ_s	σ_s	L_s	U_s
Dots	1.00	23.93	0.00	50.00	0.00	50.00	0.00	0.000	0.000	0.000	0.000
Small skew	18.00	23.67	0.82	50.01	0.06	49.99	0.08	0.000	0.002	−0.003	0.003
Medium skew	18.00	23.89	0.83	49.99	0.07	49.99	0.06	0.002	0.335	−0.659	0.735
Large skew	18.00	24.09	0.88	50.01	0.06	50.03	0.06	0.000	0.835	−0.986	0.986
Symmetric shape	18.00	24.80	0.50	49.50	0.00	49.87	0.69	0.000	0.000	0.000	0.000

where,

Number of shapes	N
Mean area (square arc-min) of set	μ_a
S.D. of area (square arc-min) in set	σ_a
Mean centroid—X coordinate in set	μ_{cx}
S.D. of centroid—X in set	σ_{cx}
Mean centroid—Y corordinate in set	μ_{cy}
S.D. of centroid—Y coordinate in set	σ_{cy}
Mean skew if set	μ_s
S.D. of skew in set	σ_s
Minimum skew in set	L_s
Maximum skew in set	U_s
One pixel	6.91 arc-sec

References

Andrews, D. P., Butcher, A. K., & Buckley, B. R. (1973). Acuities for spatial arrangement in line figures: human and ideal observers compared. *Vision Research*, *13*, 599–620.

Badcock, D. R., Hess, R. F., & Dobbins, K. (1996). Localization of element clusters: multiple cues. *Vision Research*, *36*, 1467–1472.

Bocheva, N., & Yakimoff, N. (1996). Different mechanisms may underlie the performance in relative localization tasks. *Vision Research*, *36*, 2531–2535.

Burbeck, C. A. (1987). Position and spatial frequency in large scale localization judgements. *Vision Research*, *27*, 417–428.

Hess, R. F., & Hayes, A. (1993). Neural recruitment explains 'Weber's law' of spatial position. *Vision Research*, *33*, 1673–1684.

Hess, R. F., Dakin, S. R., & Badcock, D. (1994). Localization of element clusters by the human visual system. *Vision Research*, *34*, 2439–2451.

Hess, R. F., & Holliday, I. (1996). Primitives used in spatial localization of nonabutting stimuli: peaks or centroids. *Vision Research*, *36*, 3821–3826.

Jiang, B. C., & Levi, D. M. (1991). Spatial-interval discrimination in two-dimensions. *Vision Research*, *31*, 1931–1937.

Levi, D. M., & Waugh, S. J. (1996). Position acuity with opposite-contrast polarity features: evidence for a nonlinear collector mechanism for position acuity. *Vision Research*, *36*, 573–588.

Levine, M. D. (1985). *Vision in man and machine*. New York: McGraw-Hill.

McKee, S. P. (1991). *Vision and visual dysfunction* (5). Boca Raton: CRC.

Meer, P., & Zeevi, Y. (1989). The role of stimulus structure in spatial hyperacuity. *Spatial Vision*, *4*, 141–174.

Morgan, M. J., & Aiba, T. S. (1985). Vernier acuity predicted from changes in the light distribution of the retinal image. *Spatial Vision*, *1*, 151–161.

Morgan, M. J. (1991). *Vision and visual dysfunction* (10). Boca Raton: CRC.

Morgan, M. J., & Glennerster, A. (1991). Efficiency of locating centres of dot-clusters by human observers. *Vision Research*, *31*, 2075–2083.

Mussap, A. J., & Levi, D. M. (1997). Vernier acuity with plaid masks: the role of oriented filters in vernier acuity. *Vision Research*, *37*, 1325–1340.

Press, W. H., Flannery, B. P., Teukolsky, S. A., & Vetterling, W. T. (1992). *Numerical recipes in pascal*. Cambridge: Cambridge University.

Regan, D., & Beverley, K. I. (1985). Post adaptation orientation discrimination. *Journal of the Optical Society of America A*, *2*, 147–155.

Toet, A., Smit, C. S., Nienhuis, B., & Koenderink, J. J. (1988). The visual assessment of the spatial location of a bright bar. *Vision Research*, *28*, 721–737.

Vos, P. G., Bocheva, N., Yakimoff, N., & Helsper, E. (1993). Perceived location of two-dimensional patterns. *Vision Research*, *33*, 2157–2169.

Wang, H., & Levi, D. (1994). Spatial integration in position acuity. *Vision Research*, *34*, 2859–2877.

Ward, R., Casco, C., & Watt, R. J. (1985). The location of noisy visual stimuli. *Canadian Journal of Psychology*, *39*, 387–399.

Watt, R. J. (1984). Towards a general theory of the visual acuities for shape and spatial arrangement. *Vision Research*, *24*, 1377–1386.

Waugh, S. J., Levi, D. M., & Carney, T. (1993). Orientation, masking, and vernier acuity for line targets. *Vision Research*, *12*, 1619–1638.

Waugh, S. J., & Levi, D. M. (1995). Spatial alignment across gaps: contributions of orientation and spatial scale. *Journal of the Optical Society of America A*, *12*, 2305–2317.

Westheimer, G., & McKee, S. P. (1977). Integration regions for visual hyperacuity. *Vision Research*, *17*, 89–93.

Westheimer, G., & McKee, S. P. (1977). Spatial configurations for visual hyperacuity. *Vision Research*, *17*, 941–947.

Whitaker, D., & Walker, H. (1988). Centroid evaluation in the Vernier alignment of random dot clusters. *Vision Research*, *28*, 777–784.

Whitaker, D., & McVeigh, D. (1991). Interaction of spatial frequency and separation in Vernier acuity. *Vision Research*, *31*, 1205–1212.

Whitaker, D., McGraw, P. V., Pacey, I., & Barrett, B. T. (1996). Centroid analysis predicts visual localization of first- and second-order stimuli. *Vision Research*, *36*, 2957–2970.

Wilson, H. (1986). Responses of spatial mechanisms can explain hyperacuity. *Vision Research*, *26*, 453–469.

Wilson, H. (1991). *Vision and visual dysfunction* (10). Boca Raton: CRC.

Yakimoff, N., Bocheva, N., & Mitrani, L. (1990). Perceiving the center of irregular contour quadrangles. *Spatial Vision*, *5*, 51–57.